Chinese Chemical Letters 35 (2024) 108240

Contents lists available at ScienceDirect

Chinese Chemical Letters

journal homepage: www.elsevier.com/locate/cclet

NO_x reduction against alkali poisoning over $Ce(SO_4)_2$-V_2O_5/TiO_2 catalysts by constructing the Ce^{4+}–SO_4^{2-} pair sites

Shuangxi Li, Huijun Yu, Tianwei Lan, Liyi Shi, Danhong Cheng, Lupeng Han*, Dengsong Zhang*

State Key Laboratory of Advanced Special Steel, School of Materials Science and Engineering, International Joint Laboratory of Catalytic Chemistry, College of Sciences, Shanghai University, Shanghai 200444, China

ARTICLE INFO

Article history:
Received 7 December 2022
Revised 11 January 2023
Accepted 4 February 2023
Available online 23 February 2023

Keywords:
Air pollution control
Selective catalytic reduction
NO_x reduction
Alkali poisoning
$Ce(SO_4)_2$

ABSTRACT

Commercial V_2O_5-based catalysts have been successfully applied in NH_3 selective catalytic reduction (NH_3-SCR) of NO_x from power stations, but their poor alkali-resistance restrains the wider application in nonelectrical industries. In this study, NO_x reduction against alkali poisoning over V_2O_5/TiO_2 is greatly improved *via* $Ce(SO_4)_2$ modification. It has been originally demonstrated that Ce^{4+}–SO_4^{2-} pair sites play crucial roles in improving NO_x reduction against alkali poisoning over V_2O_5/TiO_2 catalysts. The strong interaction between V species and Ce sites of Ce^{4+}–SO_4^{2-} pairs triggers the reaction between NH_4^+species and gaseous NO *via* Eley-Rideal (E-R) reaction pathway. After K-poisoning, the SO_4^{2-} sites of Ce^{4+}–SO_4^{2-} pairs as protective sites strongly bond with K and thus maintain the high reaction efficiency *via* the E-R reaction pathway. This work demonstrates an effective strategy to enhance NO_x reduction against alkali poisoning over catalysts *via* constructing Ce^{4+}–SO_4^{2-} pair sites, contributing to developing alkali-resistant SCR catalysts for practical application in nonelectrical industries.

NO_x emissions from industries and vehicles not only impair human health but also cause serious environmental issues such as PM 2.5 and O_3 [1–3]. NO_x from power plants could be effectively reduced by NH_3 selective catalytic reduction (NH_3-SCR) using V_2O_5-WO_3/TiO_2 catalysts [4–6]. Although commercial V_2O_5-based catalysts have excellent activity and SO_2 resistance at high temperatures (>300 °C), the unsatisfactory alkali-resistant capacity restricts their broader applications in steel plants, biomass burning, waste incineration plants, *etc.* [7–10]. Therefore, a large number of studies have been conducted to explore effective strategies to ameliorate the alkali-resistance of catalysts.

In general, the deactivation mechanisms of alkali poisoning include the blockage of catalyst channels and the decrease in surface acidity, which diminishes the adsorption and activation of NH_3. Extensive research has been studied on the improvement of alkali tolerance *via* increasing more acidic sites. Sulfated TiO_2 and ZrO_2 improved the acidity of catalysts and thus effectively improved alkali resistance [11–13]. The ion-exchanged titanate nanotubes (TNTs) have a number of OH groups with adequate acid content and could neutralize the basicity of alkali. Some TNTs-based catalysts such as CeO_2-doped sulfated TNTs [14], Mo modified V-TNTs [15] and Nb-doped Ce nanotubes [16] showed excellent alkali-resistance. Furthermore, it is effective to enhance the alkali-resistance of catalysts *via* constructing alkali-trapping sites to protect active sites. It has been demonstrated that BO_3^{3-} and PO_4^{3-} as capturing sites could preferentially bond with alkali metals and protect active sites of CeO_2 and Fe_2O_3 based catalysts [17,18]. Zhou *et al.* [9] found that the SCR activity was well maintained over the K-poisoned V_2O_5/CeO_2 because the in situ constructed SO_4^{2-} sites could capture K and retain a high adsorption rate and reactivity of NH_3. $Fe_2(SO_4)_3/TiO_2$ catalysts are also highly resistant to alkali due to the protective effects of SO_4^{2-} species [19]. The reactivity of K-poisoned catalysts could be recovered *via* SO_2 treatment because SO_2 preferred to combine with K, thus releasing the active sites poisoned by K [6]. These results demonstrated the protective effects of SO_4^{2-} species against alkali-poisoning. Recently, we found that Ce^{4+}–SO_4^{2-} pair sites on S doped CeO_2 catalysts not only increased the Brønsted acid sites but also greatly improved the SO_2-resistance of catalysts resulting from suppressing the adsorption and oxidation of SO_2. It is promising to develop alkali-resistant catalysts by constructing Ce^{4+}–SO_4^{2-} pair sites, which is of significance to the practice application of catalysts in complex working conditions.

In this study, we demonstrated that $Ce(SO_4)_2$ modified V_2O_5/TiO_2 (denoted as CeSV/Ti) catalysts exhibited improved NO_x

* Corresponding authors.
E-mail addresses: lphan@shu.edu.cn (L. Han), dszhang@shu.edu.cn (D. Zhang).

https://doi.org/10.1016/j.cclet.2023.108240
1001-8417/

reduction against alkali poisoning than V_2O_5/TiO_2 (denoted as V/Ti). K poisoned V/Ti showed poor activity with NO_x conversion below 70%. In comparison, K-poisoned CeSV/Ti showed much higher activity with NO_x conversion above 80% within ~270–450 °C. For revealing the promoting effects of $Ce(SO_4)_2$ on the K-resistant capacity of V/Ti catalysts, the structure features of catalysts are investigated by X-ray diffraction (XRD); the acidic amounts of catalysts were determined by NH_3 temperature-programmed desorption combined with online mass spectrum (NH_3-TPD-MS), and redox properties probed of H_2 temperature-programmed reduction (H_2-TPR), X-ray photoelectron spectroscopy (XPS), *etc*. In addition, the adsorption and activation of NH_3 and NO as well as the pathways were deeply investigated by *in situ* diffuse reflectance infrared fourier transform spectra (DRIFTS).

The catalysts were prepared *via* an impregnation method. Take the preparation of 10 wt% $Ce(SO_4)_2$ modified V_2O_5/TiO_2 catalyst as an example. First, 2 g of TiO_2 was dispersed in 10 mL of deionized water and sonicated for 5 min. 0.2 g $Ce(SO_4)_2$ and 0.051 g NH_4VO_3 were dissolved in 6 mL of deionized by a heating method, respectively. After the mixed solution was cooled, the $Ce(SO_4)_2$ solution was added by drop to the TiO_2 suspension and stirred for 1 h and then the NH_4VO_3 solution was added by drop. After stirring for 30 min, the samples are dehydrated using a rotary evaporator and then dried overnight in an oven at 80 °C. After the dried sample was calcined in a muffle furnace at 450 °C for 4 h with a ramping rate of 2 °C/min, 10 wt% $Ce(SO_4)_2$ modified V_2O_5/TiO_2 was obtained, named as CeSV/Ti. Other 5, 15 and 20 wt% $Ce(SO_4)_2$ modified V_2O_5/TiO_2 catalysts were prepared using the same method. The Ce^{4+}-modified and SO_4^{2-}-modified V/Ti catalysts were prepared by impregnating 0.2614 g of $Ce(NO_3)_3{\cdot}6H_2O$ and 0.1591 g of $(NH_4)_2SO_4$, respectively. The preparation of V_2O_5/TiO_2 catalysts is similar to CeSV/Ti without the addition of $Ce(SO_4)_2$, named as V/Ti. K-poisoned CeSV/Ti and V/Ti catalysts were prepared by the impregnation method. 0.017 g of KNO_3 was dissolved in 10 mL of deionized water, and 0.5 g CeSV/Ti and V/Ti catalysts were added and stirred for 1 h. The mixture was dehydrated by a rotary evaporator, dried overnight in an oven at 80 °C, and then calcined in a muffle furnace under 450 °C for 4 h with a ramping rate of 2 °C/min. The obtained catalysts were named as K-CeSV/Ti and K-V/Ti, respectively. Characterizations of the obtained catalysts can be found in Supporting information.

SCR activity was characterized by using a fixed-bed quartz flow reactor (inner diameter: 8 mm) with the catalyst (40–60 meshes). SCR activity was tested from 150 °C to 420 °C. The gas mixture composition: 500 ppm of NO, 500 ppm of NH_3, 5 vol% of O_2, and N_2 as the balance gas. The gas hourly space velocity (GHSV) was controlled at 50,000 h^{-1} corresponding to the total flow rate of 257.7 mL/min. FTIR spectrometer (Protea atmosFIR) was used to simultaneously monitor the concentrations of NO, NO_2, NH_3, H_2O, and N_2O. The SCR activity data were recorded after the reaction system reached a stable state.

The NO_x conversion, N_2 selectivity, and GHSV were calculated by using the following formulas:

$$NO_x\ \text{conversion}(\%) = \frac{[NO_x]_{in} - [NO_x]_{out}}{[NO_x]_{in}} \times 100\%$$

$$N_2\ \text{selectivity}(\%) = \left(1 - \frac{2[N_2O]_{out} + [NO_2]_{out}}{[NO_x]_{in} + [NO_3]_{in} - [NO_x]_{out} - [NH_3]_{out}}\right) \times 100\%$$

where NO_x represents the total concentration of NO and NO_2. $[NO_x]_{in}$, $[NO_x]_{out}$, $[N_2O]_{out}$, $[NH_3]_{in}$, and $[NH_3]_{out}$ stood for the inlet and outlet concentrations of corresponding gas, respectively.

The GHSV was calculated by the following equation: $GHSV = q_v/\pi hr^2 q_v$ meant the total flow rate; h represented the height of the catalyst in the reactor; and r stood for the inner radius of the reactor.

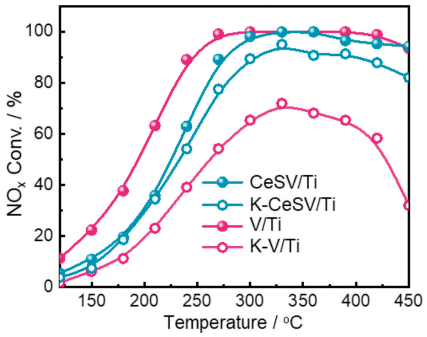

Fig. 1. Plots of NO_x conversion *versus* temperature over CeSV/Ti, K-CeSV/Ti, V/Ti and K-V/Ti catalysts. Reaction conditions: 500 ppm NO, 500 ppm NH_3, 5 vol% O_2, N_2 as the balance gas, and GHSV of 50,000 h^{-1}.

Firstly, the SCR activities of fresh and K-poisoned V/Ti catalysts were tested, while different amounts of $Ce(SO_4)_2$ modified V/Ti catalysts were compared (Figs. S1 and S2 in Supporting information). It can be seen that V/Ti shows NO_x conversion above 90% within 240–450 °C (Fig. 1 and Fig. S1). Different amounts of $Ce(SO_4)_2$ modified V/Ti catalysts all show decreased activities to some extent, in which 10–15 wt% $Ce(SO_4)_2$ modified ones show satisfactory activity with NO_x conversion above 90% from 270 °C to 450 °C. After K-poisoning, the activity of K-V/Ti decreases markedly with the highest NO_x conversion of only 72% at 330 °C (Fig. 1 and Fig. S2). For K-poisoned $Ce(SO_4)_2$ modified V/Ti catalysts, the activity increases and then decreases with increasing $Ce(SO_4)_2$ amount from 5 wt% to 20 wt%, and the 10 wt% $Ce(SO_4)_2$ modified V/Ti exhibits the highest activity with NO_x conversion above 90% from 300 °C to 450 °C (Fig. 1). Besides, the fresh and K-poisoned CeSV/Ti show good N_2 selectivity above 95% (Fig. S3 in Supporting information). The CeSV/Ti catalyst exhibits excellent H_2O tolerance at 300 °C (Fig. S4 in Supporting information). Clearly, $Ce(SO_4)_2$ modification notably improves NO_x reduction against alkali poisoning over V/Ti catalysts. The $Ce(SO_4)_2$ amount more than 10 wt% may led to the poor dispersion of $Ce(SO_4)_2$, that is unfavorable for the alkali resistance. Besides, we also supplemented the SCR activity for Ce^{4+}-modified and SO_4^{2-} modified V/Ti catalysts and their K-poisoned ones (Fig. S3). Although the low-temperature activities of CeV/Ti and SV/Ti are better than that of CeSV/Ti, the activity of K-poisoned CeSV/Ti is higher than that of K-poisoned CeV/Ti and SV/Ti catalysts. These results indicate that Ce^{4+}–SO_4^{2-} pair sites play crucial roles in the strong alkali resistance of CeSV/Ti.

Firstly, the thermal stability of CeSV/Ti catalyst was tested *via* the N_2 temperature-programmed decomposition (TPDC (Fig. S5 in Supporting information). A small quantity of SO_2 ($m/z = 64$) was detected below 500 °C that is derived from the decomposition of surface adsorbed SO_4^{2-} species. The decomposition peak of $Ce(SO_4)_2$ occurs above 500 °C associated with the large formation of SO_2. The thermogravimetry (TG) analysis also shows the similar results (Fig. S6 in Supporting information). These results indicate the good thermal stability of CeSV/Ti within the temperature range of the activity test of catalysts. In order to probe the nature reason for the stronger alkali-resistance of CeSV/Ti catalysts, the structure features of fresh and K-poisoned CeSV/Ti and V/Ti catalysts were investigated by XRD (Fig. S7 in Supporting information). All catalysts display characteristic diffraction peaks ascribed to anatase TiO_2 (PDF #21–1272). There are no characteristic diffraction peaks related to Ce and V species, implying the highly dispersed state of Ce and V species. From the N_2 adsorption-desorption isotherm, all fresh and K-poisoned catalysts show mesoporous features due

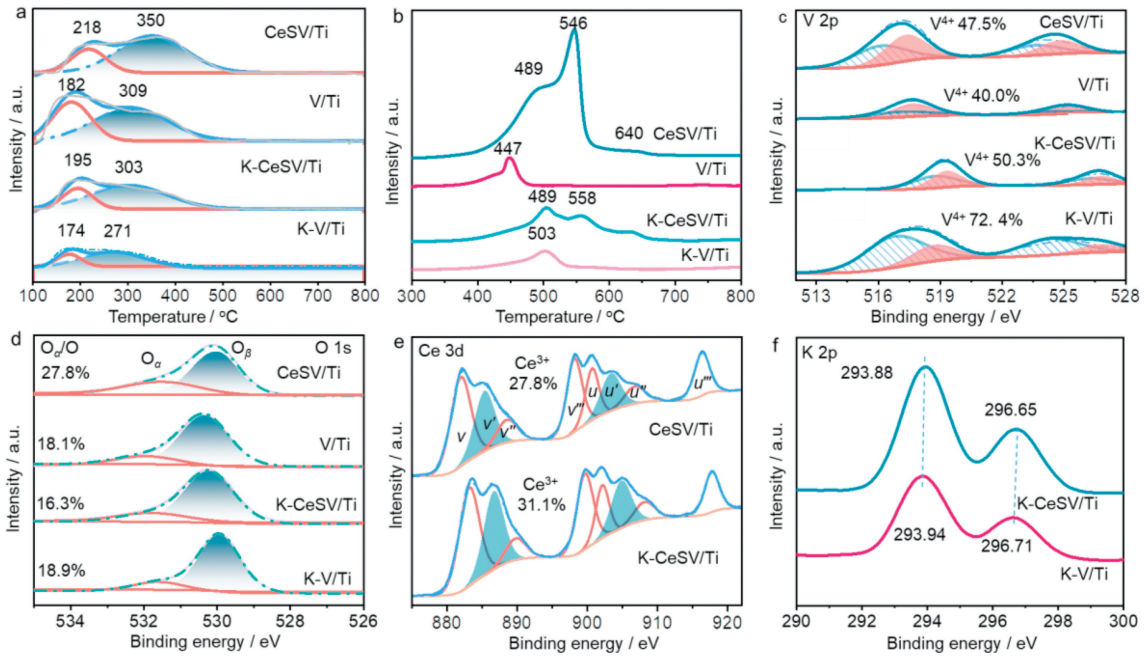

Fig. 2. (a) NH_3-TPD-MS profiles; (b) H_2-TPR profiles; XPS spectra of V 2p (c), O 1s (d), Ce 3d (e) and K 2p (f) of different catalysts.

to the unique capillary adsorption phenomenon (Figs. S8–S11 in Supporting information). It can be seen that the pore volumes and pore sizes of both K-poisoned catalysts decrease compared to the fresh ones (Table S1 in Supporting information), indicating that the K_2O nanoparticles enter the pore channels and occupy partial space of pores of fresh catalysts. However, the specific surface areas of CeSV/Ti and V/Ti catalysts both increase to some extent after K-poisoning, which is likely owing to that K_2O nanoparticles in the pore channels contribute to the specific surface areas. Besides, the pore volume and pore diameter of catalysts both decrease to some extent after K-poisoning, which results from that K_2O nanoparticles occupy the partial position of pores surface. These results indicate that there are no correlations between textual features and the activity of catalysts.

Acid sites of catalysts play crucial roles in NH_3 adsorption/activation, and NH_3-TPD-MS was performed to study the acidic properties of fresh and K-poisoned catalysts. As shown in Fig. 2a, both CeSV/Ti and V/Ti catalysts show two NH_3 desorption peaks, where the low-temperature peaks are attributed to the weak acid sites and the high-temperature one ascribed to strong acid sites, respectively [20,21]. It is notable that the total acid amount of V/Ti increases from 20.2 μmol/g to 26.0 μmol/g after $Ce(SO_4)_2$ modification. After K-poisoning, the total acid amount of K-CeSV/Ti and K-V/Ti both decreases to some extents. The total acid amount (12.0 μmol/g) of K-CeSV/Ti is higher than that (7.4 μmol/g) of K-V/Ti (Table S2 in Supporting information), which contributes to the SCR activity of K-CeSV/Ti. The reducibility of fresh and K-poisoned CeSV/Ti and V/Ti catalysts were probed by H_2-TPR. As shown in Fig. 2b, the reduction peak at 447 °C on V/Ti is attributed to the reduction of VO_x species. For CeSV/Ti, the reduction peak at 489 °C is ascribed to the reduction of VO_x and Ce^{4+} species while the peaks at 546 and 640 °C are related to the reduction of SO_4^{2-} species [22]. Compared with V/Ti, the higher reduction temperature of V species over CeSV/Ti indicates the strong interaction between Ce and V. After K-poisoning, the reduction peak of VO_x species shifts to a higher temperature of 503 °C for K-V/Ti, indicating the K bonded VO_x species become more difficult to reduce. The reduction temperatures of VO_x, Ce^{4+} and SO_4^{2-} species over K-CeSV/Ti have no large changes compared with CeSV/Ti. However, it is notable that the reduction peak intensity of Ce^{4+} and SO_4^{2-} species markedly reduces over the K-poisoned CeSV/Ti, implying that SO_4^{2-} species as sacrificial sites bond with K.

To investigate the redox properties of fresh and K-poisoned catalysts, XPS was applied to probe the electron states of V and O on the surface of catalysts. As shown in Fig. 2c, the XPS spectra of V 2p show two characteristic binding energies of V $2p_{3/2}$ and V $2p_{1/2}$, where the peaks around 516 and 524 eV are attributed to V^{4+} species while the peaks around 517 and 525 eV are ascribed to V^{5+} [23]. It can be found that the $V^{4+}/(V^{4+}+V^{5+})$ ratio (47.5%) on CeSV/Ti is higher than that (40.0%) on V/Ti, evidencing the strong interaction between Ce and V species over CeSV/Ti. The lower valence of V over CeSV/Ti indicates that the electron could transfer from Ce to V. After K-poisoning, the $V^{4+}/(V^{4+}+V^{5+})$ of K-V/Ti increases markedly to 72.4% while that (50.3%) of K-CeSV/Ti hardly changes compared to the fresh catalysts. The significant increase in V^{4+} fraction of K-V/Ti is attributed to the electron-donating effects of K that increase the electron density of V species. This also demonstrates that K strongly interacts with V species after K-poisoning. Differently, the maintenance of V valence over K-CeSV/Ti implies that K strongly interacts with $Ce(SO_4)_2$ rather than V. The O 1s XPS spectra were used to investigate the varieties and contents of surface oxygen species. The surface oxygen atomic percent (53.8%) of CeSV/Ti is much higher than that (27.0%) of V/Ti, which is attributed to the oxygen species of $Ce(SO_4)_2$ (Table S3 in Supporting information). After K-poisoning, the surface oxygen atomic percent of K-CeSV/Ti slightly decreases to 46.5% while that of K-V/Ti increases to 45.6%. These results imply that K_2O is mainly bonded on $Ce(SO_4)_2$ sites of K-CeSV/Ti but cover on the surface of K-V/Ti. As shown in Fig. 2d, there are adsorbed oxygen (O_α) species around 531 eV and lattice oxygen (O_β) species around 530 eV [24–31]. $Ce(SO_4)_2$ modification increases the O_α fraction of V/Ti from 18.1% to 27.8%, likely due to the contribution of surface SO_4^{2-}. After K-poisoning, the O_α species of K-CeSV/Ti decrease notably to 16.3% while that of K-V/Ti keeps unchanged at 18.9%, respectively. It can be inferred that SO_4^{2-} of $Ce(SO_4)_2$ strongly interacts with K over K-CeSV/Ti, which leads to the decrease of O_α species. By the contrast, K_2O covers on the surface of K-V/Ti that results in

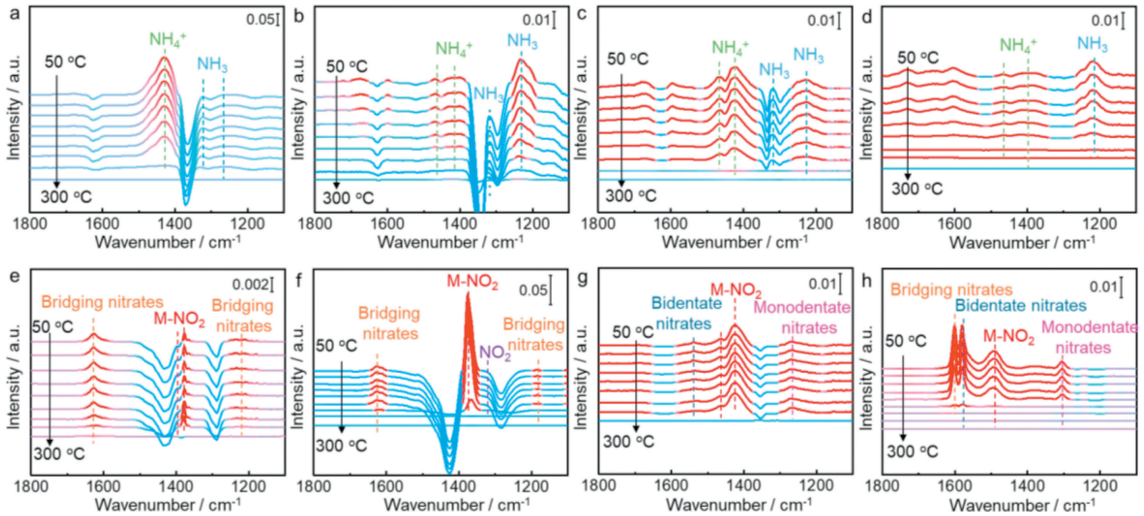

Fig. 3. *In situ* DRIFTS of NH_3 desorption over CeSV/Ti (a), V/Ti (b), K-CeSV/Ti (c), and K-V/Ti (d) catalysts after exposure to NH_3 for 1 h at 30 °C; *In situ* DRIFTS of $NO+O_2$ desorption over CeSV/Ti (e), V/Ti (f), K-CeSV/Ti (g), and K-V/Ti (h) catalysts after exposure to $NO+O_2$ for 1 h at 30 °C. The spectra were all recorded at 50, 80, 110, 140, 170, 200, 230, 260 and 300 °C, respectively.

the unchanged amount of O_α species because of the O_α species of K_2O. In order to probe the interaction between Ce and K species on the K-CeSV/Ti catalysts, the XPS spectra of Ce 3d and K 2p are investigated over CeSV/Ti, K-CeSV/Ti and K-V/Ti catalysts (Figs. 2e and f). The peaks labelled as *v*, *v*″, *v*‴, *u*, *u*″ and *u*‴ at 882, 888.9, 898, 901, 907 and 916.8 eV are attributed to the $3d^{10}4f^0$ Ce^{4+} state, while the peaks labeled *v*′ and *u*′ observed at 885 and 903 eV are ascribed to the $3d^{10}4f^1$ Ce^{3+} state (Fig. 2e) [28]. It can be found that the ratio of $Ce^{3+}/(Ce^{3+}+Ce^{4+})$ (31.1%) of K-CeSV/Ti is higher than that (27.8%) of CeSV/Ti, indicating the more electron-rich state of Ce in K-CeSV/Ti. On the other hand, the XPS spectra of K 2p were also investigated over K-CeSV/Ti and K-V/Ti catalysts. As seen in Fig. 2f, the binding energy of K on K-CeSV/Ti is higher than that on K-V/Ti, indicating the electron deficient state of K on the former one. Based on these results, it can be inferred that K is bonded on $Ce(SO_4)_2$ sites, leading to the transfer of electron from K to Ce species.

To explore the effects of K-poisoning on the adsorption and activation behavior of NH_3 and NO_x, the *in situ* DRIFTS of adsorption and desorption for NO_x and NH_3 species were investigated over fresh and poisoned catalysts. As shown in Fig. 3a, after introducing NH_3, the band at 1429 cm^{-1} [32] ascribed to NH_4^+ and the bands around 1324 [33] and 1257 cm^{-1} [34] ascribed to NH_3 species are observed on CeSV/Ti catalysts. These NH_3/NH_4^+ species gradually decrease and disappear above 300 °C with increasing the desorption temperature. Similarly, the NH_3 species (1328 and 1229 cm^{-1}) [33,35] and NH_4^+ species (1470 and 1411 cm^{-1}) [36,37] appear on V/Ti after the adsorption of NH_3 (Fig. 3b). With the increasing desorption temperature, the NH_3/NH_4^+ species gradually decrease and disappear above 300 °C. Notably, there are more NH_4^+ species on CeSV/Ti catalysts and a larger number of NH_3 species on V/Ti catalysts. After K-poisoning, the adsorption amount of NH_3/NH_4^+ species both decrease on K-CeSV/Ti and K-V/Ti catalysts compared with the fresh catalysts. As seen in Fig. 3c, the NH_3 species (1228 and 1321 cm^{-1}) [33,35] and NH_4^+ species (1423 and 1467 cm^{-1}) [38,39] appear on K-CeSV/Ti after the adsorption of NH_3. These NH_3/NH_4^+ species decrease and disappear above 260 °C with increasing the desorption temperature. As for K-V/Ti (Fig. 3d), NH_3 species (1217 cm^{-1}) [40] and NH_4^+ species (1398 and 1468 cm^{-1}) [36,41] appear after the adsorption of NH_3. With increasing desorption temperature, these NH_3/NH_4^+ species decrease and disappear above 230 °C. These results imply that the adsorption strength of NH_4^+ species on K-CeSV/Ti is stronger than that of NH_3 species on K-V/Ti.

As shown in Fig. 3e, the adsorbed NO_x species such as the bridging nitrate species (1626 and 1225 cm^{-1}) and M-NO_2 (1379 cm^{-1}) appear on CeSV/Ti after the adsorption of $NO+O_2$ [42]. With increasing desorption temperature, these NO_x species gradually decrease and disappear above 300 °C. As for V/Ti (Fig. 4f), the bridging nitrate species (1624 and 1183 cm^{-1}), M-NO_2 (1375 cm^{-1}) and gaseous NO_2 species (1324 cm^{-1}) appear after the adsorption of $NO+O_2$ [42]. These NO_x species decrease and disappear above 260 °C with increasing the desorption temperature. It is notable that the amount of NO_x species over V/Ti is much higher than that over CeSV/Ti. Besides, the NO_x species adsorbed much more strongly on CeSV/Ti than that on V/Ti, implying that these NO_x species on CeSV/Ti are not easy to participate in the SCR reaction. Therefore, the SCR reaction may occur on the CeSV/Ti catalyst between the adsorbed NH_x species and gaseous NO following the Eley-Rideal (E-R) mechanism while the reaction might procced between the adsorbed NH_x and NO_x species following the Langmuir-Hinshelwood (L-H) mechanism over V/Ti. After K-poisoning, the adsorption strength of NO_x species changes compared to fresh catalysts. As shown in Fig. 4g, the bidentate nitrate species (1543 cm^{-1}), M-NO_2 (1423 and 1466 cm^{-1}) and monodentate nitrates (1264 cm^{-1}) appear on K-CeSV/Ti after the adsorption of $NO+O_2$ [42]. The amount of these NO_x species is much more than that on fresh CeSV/Ti while these NO_x species adsorb strongly and only disappear above 300 °C with increasing the desorption temperature. This result implies that K-poisoning improves the adsorption of NO_x species but these species are relatively inactive. The reaction might still follow between NH_4^+ species and gaseous NO *via* the E-R mechanism over K-CeSV/Ti. As for K-V/Ti (Fig. 4h), the bridging nitrate species (1601 cm^{-1}), bidentate nitrate species (1582 cm^{-1}), M-NO_2 (1493 cm^{-1}) and monodentate nitrates (1307 cm^{-1}) appear after the adsorption of $NO+O_2$ [42]. The amount of these NO_x species is much less than fresh V/Ti. With the increase of desorption temperature, these NO_x species decrease and disappear above 200 °C. This result implies that K-poisoning impairs the adsorption of NO_x species and the reaction might also occur between NH_4^+ species and NO_x species *via* the L-H mechanism over K-V/Ti.

To further explore the alkali-resistant mechanism, *in situ* DRIFT spectra of transient reactions were performed at 200 °C. Firstly,

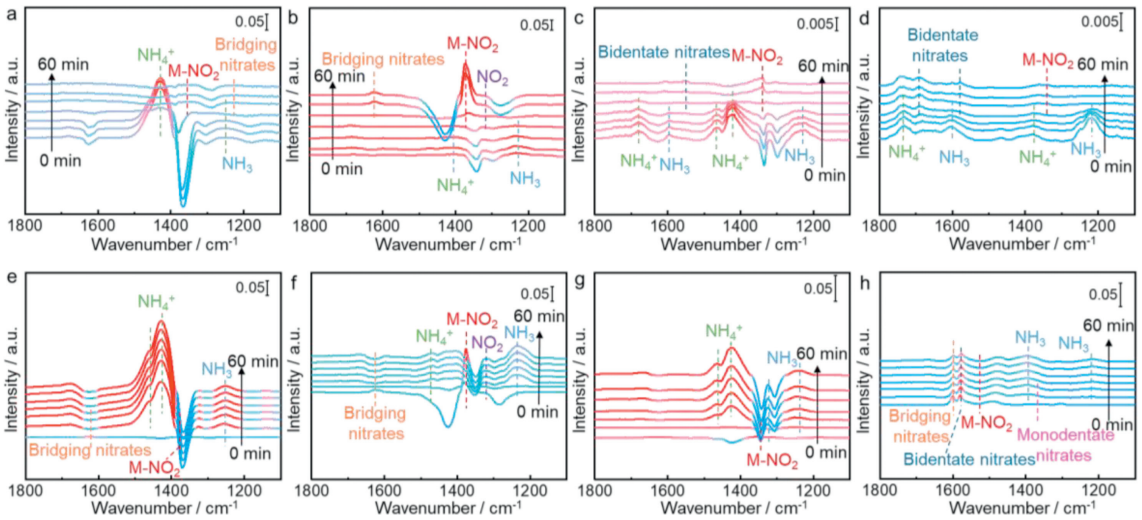

Fig. 4. *In situ* DRIFTS of the transient reactions between NO+O_2 and pre-adsorbed NH_3 over CeSV/Ti (a), V/Ti (b), K-CeSV/Ti (c), and K-V/Ti (d) catalysts at 200 °C as a function of time; *In situ* DRIFTS of the transient reactions between NH_3 and pre-adsorbed NO+O_2 over CeSV/Ti (e), V/Ti (f), K-CeSV/Ti (g), and K-V/Ti (h) catalysts at 200 °C as a function of time. The spectra were all recorded at 0, 10, 20, 30, 40, 50, and 60 min, respectively.

the *in situ* DRIFT spectra of transient reactions between NO+O_2 and pre-adsorbed NH_3 were probed for fresh catalysts, as shown in Figs. 4a and b. As for CeSV/Ti (Fig. 4a), the NH_4^+ (1428 cm^{-1}) [43] and NH_3 (1249 cm^{-1}) [44] species appear after the adsorption of NH_3, in which the amount of NH_4^+ species is more than NH_3 species. With the introduction of NO+O_2, these NH_3/NH_4^+ species gradually decrease within 20 min and a small quantity of nitrates including M-NO_2 nitrate species (1346 cm^{-1}) and bridging nitrate (1237 cm^{-1}) emerged [42]. For V/Ti (Fig. 4b), the NH_3 species (1233 cm^{-1}) [44] and NH_4^+ species (1418 cm^{-1}) [45] appear after the adsorption of NH_3, where the amount of NH_3 species is more than NH_4^+ species. With the introduction of NO+O_2, these NH_3/NH_4^+ species consume gradually within 40 min, and the M-NO_2 (1373 cm^{-1}), bridging species (1623 cm^{-1}) and gaseous NO_2 (1320 cm^{-1}) increase [42]. It is notable that more NH_3/NH_4^+ species are generated over CeSV/Ti than V/Ti. Besides, the reactivity of NH_3/NH_4^+ species over CeSV/Ti is also higher than that on V/Ti. Figs. 4c and d show the in situ DRIFT spectra of transient reactions for K-poisoned catalysts between NO+O_2 and pre-adsorbed NH_3 at 200 °C. As for K-CeSV/Ti (Fig. 4c), the NH_3 species (1230 and 1595 cm^{-1}) [38,44] and NH_4^+ species (1418, 1470 and 1684 cm^{-1}) [36,45,46] appear after the adsorption of NH_3. Similar to the fresh CeSV/Ti, the amount of NH_4^+ species is still more than NH_3 species. With the introduction of NO+O_2, these NH_3/NH_4^+ species gradually decrease and a small quantity of bidentate nitrates species (1551 cm^{-1}) and M-NO_2 species (1340 cm^{-1}) emerge [42]. For K-V/Ti (Fig. 4d), the NH_3 species (1217 and 1603 cm^{-1}) [37,40] and NH_4^+ species (1732 and 1379 cm^{-1}) [43,47] appear after the adsorption of NH_3. Meanwhile, the amount of NH_3 species is more than NH_4^+ species. With the introduction of NO+O_2, these NH_3/NH_4^+ species gradually decrease while the bidentate nitrates species (1579 cm^{-1}) and M-NO_2 species (1359 cm^{-1}) gradually emerge [42]. Clearly, the adsorption of NO_x species on V/Ti catalysts is much stronger than CeSV/Ti, indicating that the gaseous NO mainly participates the SCR reaction over CeSV/Ti catalysts.

Figs. 4e and f show *in situ* DRIFT spectra of the transient reactions at 200 °C between NH_3 and pre-adsorbed NO+O_2 for fresh catalysts. For CeSV/Ti (Fig. 4e), a small quantity of bridging nitrate species (1626 cm^{-1}) and M-NO_2 (1381 cm^{-1}) appear after the adsorption of NO+O_2 [42]. With the introduction of NH_3, these adsorbed NO_x species decrease while the NH_4^+ species (1469 and 1429 cm^{-1}) [36,48] and NH_3 species (1250 cm^{-1}) [34] gradually increase. From the above results, it can be inferred that the reaction mainly proceeds between NH_4^+ species and gaseous NO *via* the E-R reaction pathway over CeSV/Ti. For V/Ti (Fig. 4f), the bridging nitrates (1628 cm^{-1}), M-NO_2 species (1377 cm^{-1}) and adsorbed NO_2 (1320 cm^{-1}) appear after the adsorption of NO+O_2 [42]. After the introduction of NH_3, these NO_x species gradually decrease while the NH_3 species (1235 cm^{-1}) [44] and NH_4^+ (1468 and 1410 cm^{-1}) [36,37] increase. Based the above results, the reaction mainly proceeds between NH_3 species and NO_x species *via* the L-H reaction pathway over V/Ti.

Figs. 4g and h show the *in situ* DRIFTS of transient reactions for K poisoned-catalysts between NH_3 and pre-adsorbed NO+O_2 at 200 °C. As for K-CeSV/Ti (Fig. 4g), only a small quantity of M-NO_2 species (1338 cm^{-1}) are detected after the adsorption of NO+O_2 [42]. With introduction of NH_3, these NO_x species were consumed within 10 min and corresponding NH_3 (1324 and 1237 cm^{-1}) [33] and NH_4^+ (1421 and 1466 cm^{-1}) [39,49] species gradually increase. Therefore, the SCR reaction could still proceed *via* the reaction between NH_4^+ species and gaseous NO over K-CeSV/Ti (Fig. 4). For K-V/Ti (Fig. 4h), the bridging nitrates (1601 cm^{-1}), bidentate nitrates (1578 cm^{-1}), M-NO_2 (1484 cm^{-1}) and monodentate nitrates (1307 cm^{-1}) species are accumulated after the adsorption of NO+O_2 over the K-poisoned V/Ti [42]. However, after the introduction of NH_3, these NO_x species consumed slowly while the NH_3 species (1397 and 1219 cm^{-1}) [40,49] are detected. This result indicates that K-poisoning decreases the reactivity of the adsorbed NO_x with NH_3 species and blocked the L-H reaction pathway (Fig. 4).

In summary, improved NO_x reduction against alkali poisoning over CeSV/Ti catalysts has been originally demonstrated. K poisoned V/Ti shows NO_x conversion below 70% while K-poisoned CeSV/Ti shows NO_x conversion above 80% from 270 °C to 450 °C. It has been demonstrated that Ce^{4+}–SO_4^{2-} pair sites play crucial roles in improving the K-resistance of V/Ti catalysts. Here, we propose a deactivation mechanism over K-V/Ti and alkali-resistant mechanism over K-CeSV/Ti catalysts, as seen in Fig. 5. V/Ti catalysts mainly proceed the reaction between NH_3 species and NO_x species *via* the L-H reaction pathway. After $Ce(SO_4)_2$ modification, the strong interaction between V and Ce sites of Ce^{4+}–SO_4^{2-} pair leads to the change of L-H reaction pathway into the E-R reaction pathway *via* the reaction between NH_4^+ species and gaseous NO. After K-poisoning, the reactivity between the adsorbed NO_x

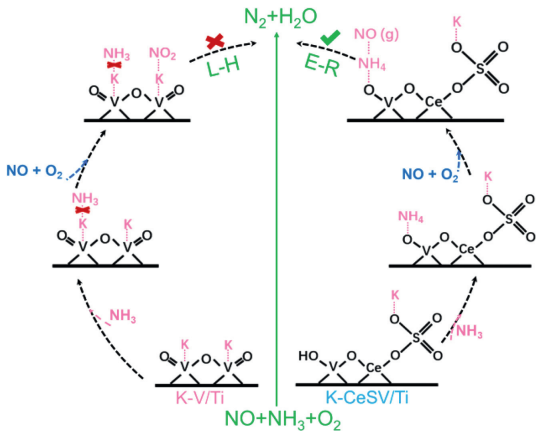

Fig. 5. Schematic diagram of the deactivation mechanism over K-V/Ti and alkali-resistant mechanism over K-CeSV/Ti catalysts.

species and NH_3 species is impaired over K-V/Ti and thus the L-H reaction pathway is blocked. In comparison, K-CeSV/Ti could still proceed the reaction effectively *via* the E-R reaction pathway because the SO_4^{2-} sites of Ce^{4+}–SO_4^{2-} pairs strongly bond with K and protect active sites. This work evidenced an effective strategy to enhance NO_x reduction against alkali poisoning over catalysts *via* constructing Ce^{4+}–SO_4^{2-} pair sites, contributing to developing alkali-resistant SCR catalysts for practical application in nonelectrical industries.

Declaration of competing interest

The authors declare that they have no known competing financial interests or personal relationships that could have appeared to influence the work reported in this paper.

Acknowledgments

We acknowledge the National Natural Science Foundation of China (Nos. 22125604, 22106100, 21976117), Shanghai Rising-Star Program (No. 22QA1403700) and Chenguang Program supported by Shanghai Education Development Foundation and Shanghai Municipal Education Commission (No. 22Z00354).

Supplementary materials

Supplementary material associated with this article can be found, in the online version, at doi:10.1016/j.cclet.2023.108240.

References

[1] A. Richter, J.P. Burrows, H. Nüß, C. Granier, U. Niemeier, Nature 437 (2005) 129–132.
[2] C. Paolucci, I. Khurana, A.P. Atish, et al., Science 357 (2017) 898–903.
[3] H.K. Chang, G. Qi, K. Dahlberg, W. Li, Science 327 (2010) 1624–1627.
[4] C. Paolucci, A.A. Verma, S.A. Bates, et al., Angew. Chem., Int. Ed. 53 (2014) 11828–11833.
[5] G. He, Z. Lian, Y. Yu, et al., Sci. Adv. 4 (2018) eaau4637.
[6] Z. Si, Y. Shen, J. He, et al., Environ. Sci. Technol. 56 (2022) 605–613.
[7] L. Han, S. Cai, M. Gao, et al., Chem. Rev. 119 (2019) 10916–10976.
[8] Y. Zhao, L. Shi, Y. Shen, et al., Environ. Sci. Technol. 56 (2022) 4386–4395.
[9] G. Zhou, P. Maitarad, P. Wang, et al., Environ. Sci. Technol. 54 (2020) 13314–13321.
[10] L. Yan, Y. Ji, P. Wang, et al., Environ. Sci. Technol. 54 (2020) 9132–9141.
[11] S.S.R. Putluru, S.B. Kristensen, J. Due-Hansen, A. Riisager, R. Fehrmann, Catal. Today 184 (2012) 192–196.
[12] S. Gao, P. Wang, X. Chen, et al., Catal. Commun. 43 (2014) 223–226.
[13] J. Due-Hansen, S. Boghosian, A. Kustov, et al., J. Catal. 251 (2007) 459–473.
[14] P. Wang, H. Wang, X. Chen, Z. Wu, ChemCatChem 8 (2016) 787–797.
[15] P. Wang, S. Gao, H. Wang, et al., Appl. Catal. B 561 (2018) 68–77.
[16] P. Wang, S. Chen, S. Gao, et al., Appl. Catal. B 231 (2018) 299–309.
[17] P. Zhang, P. Wang, A. Chen, et al., Environ. Sci. Technol. 55 (2021) 11970–11978.
[18] Y. Li, S. Cai, P. Wang, et al., Environ. Sci. Technol. 55 (2021) 9276–9284.
[19] C. Feng, P. Wang, X. Liu, et al., Environ. Sci. Technol. 55 (2021) 11255–11264.
[20] L. Kang, L. Han, J. He, et al., Environ. Sci. Technol. 53 (2019) 938–945.
[21] Z. Chen, S. Ren, M. Wang, et al., Fuel 321 (2022) 124113.
[22] H. Zhou, T. Cheng, B. Du, et al., Environ. Sci. Pollut. Res. 29 (2022) 84421–84433.
[23] L. Wang, J. Zhao, S. Bai, H. Zhao, Z. Zhu, Chem. Eng. J. 254 (2014) 399–409.
[24] L. Han, M. Gao, J.Y. Hasegawa, et al., Environ. Sci. Technol. 53 (2019) 6462–6473.
[25] L. Kang, L. Han, P. Wang, et al., Environ. Sci. Technol. 54 (2020) 14066–14075.
[26] Z. Chen, S. Ren, X. Xing, et al., Fuel 335 (2022) 126986.
[27] Z. Chen, S. Ren, M. Wang, Mol. Catal. 531 (2022) 112693.
[28] L. Han, M. Gao, C. Feng, L. Shi, D. Zhang, Environ. Sci. Technol. 53 (2019) 5946–5956.
[29] Z. Liu, H. Su, B. Chen, J. Li, S.I. Woo, Chem. Eng. J. 299 (2016) 255–262.
[30] Z. Wu, R. Jin, Y. Liu, H. Wang, Catal. Commun. 9 (2008) 2217–2220.
[31] Z. Chen, R. Guo, S. Ren, et al., J. Mater. Chem. A 10 (2022) 21474.
[32] K. Wang, Z. Gong, H. Luo, et al., Combust. Sci. Technol. 190 (2018) 770–783.
[33] Y. Zhang, X. Yue, T. Huang, K. Shen, B. Lu, Materials 11 (2018) 1307.
[34] Q. Zhang, J. Fan, P. Ning, et al., Appl. Surf. Sci. 435 (2018) 1037–1045.
[35] J. Liu, J. Meeprasert, S. Namuangruk, et al., J. Phys. Chem. C 121 (2017) 4970–4979.
[36] L. Chen, Z. Si, X. Wu, D. Weng, ACS Appl. Mater. Interfaces 6 (2014) 8134–8145.
[37] Y. Yu, J. Wang, J. Chen, et al., Ind. Eng. Chem. Res. 53 (2014) 16229–16234.
[38] L. Huang, K. Zha, S. Namuangruk, et al., Catal. Sci. Technol. 6 (2016) 8516–8524.
[39] J. Liu, X. Li, Q. Zhao, et al., Appl. Catal. B 200 (2017) 297–308.
[40] Q. Zhang, H. Wang, P. Ning, et al., Appl. Surf. Sci. 419 (2017) 733–743.
[41] J. Wang, Z. Yan, L. Liu, et al., Appl. Surf. Sci. 313 (2014) 660–669.
[42] A. Davydov, Molecular Spectroscopy of Oxide Catalyst Surfaces, John Wiley & Sons Ltd., 2003, Chapter 2, p. 124.
[43] Z. Liu, S. Zhang, J. Li, L. Ma, Appl. Catal. B 144 (2014) 90–95.
[44] N. Liu, J. Wang, F. Wang, J. Liu, J. Rare Earths 36 (2018) 594–602.
[45] H. Hu, S. Cai, H. Li, et al., J. Phys. Chem. C 119 (2015) 22924–22933.
[46] C. Yu, L. Wang, B. Huang, Aerosol Air Qual. Res. 15 (2015) 1017–1027.
[47] X. Weng, X. Dai, Q. Zeng, Y. Liu, Z. Wu, J. Colloid Interface Sci. 461 (2016) 9–14.
[48] S. Wang, R. Guo, W. Pan, et al., Catal. Commun. 89 (2017) 143–147.
[49] K. Liu, F. Liu, L. Xie, W. Shan, H. He, Catal. Sci. Technol. 5 (2015) 2290–2299.